Eur. Phys. J. B **32**, 421–428 (2003)
DOI: 10.1140/epjb/e2003-00120-9

THE EUROPEAN PHYSICAL JOURNAL B

Theoretical study of electronic and positronic properties in $Ga_xIn_{1-x}P_ySb_zAs_{1-y-z}$ lattice matched to GaSb

N. Bouarissa[a]

Physics Department, University of M'sila, 28000 M'sila, Algeria

Received 30 August 2002 / Received in final form 12 February 2003
Published online 24 April 2003 –

Abstract. The electronic and positronic properties of the pentanary semiconductor alloys $Ga_xIn_{1-x}P_ySb_zAs_{1-y-z}$ lattice matched to GaSb have been studied. The electron wave function is calculated semiempirically using the pseudopotential band model under the virtual crystal approximation. The positron wave function is evaluated under the point core approximation for the ionic potential. Electronic and positronic quantities namely, electronic structure and band gaps, positron band structure, effective mass and affinity, and electron-positron momentum densities have been predicted and their dependence on the phosphorus composition has been discussed.

PACS. 71.20.-b Electron density of states and band structure of crystalline solids – 71.60.+z Positron states – 78.70.Bj Positron annihilation

1 Introduction

In recent years, efforts have been made to provide a deeper understanding of electronic properties of semiconductor alloys, with a view to improving the tunability of band structure parameters for guiding the successful design and fabrication of optoelectronic devices over a continuous broad spectrum of energies. At present, III-V compound semiconductors provide the materials basis for a number of well-established commercial technologies [1]. Their multicomponent alloys are promising candidates for many device applications such as high speed electronic and long wavelength photonic devices because their band gaps (E_0) cover a wide spectral range from ∼0.3 eV to ∼1.5 eV (*i.e.*, λ (μm)= $1.24/E_0$ (eV); 4.1−0.8 μm) [2]. Recently developed techniques for growing crystalline random alloys, such as molecular beam epitaxy (MBE), liquid phase epitaxy (LPE), and metalorganic chemical vapor deposition (MOCVD), have stimulated theoretical and experimental research on ternary and few quaternary semiconductor alloys [1–7]. However, to the best of our knowledge, no experiments for III-V multi-component semiconductor alloys, with more than two composition variables, (*i.e.*, larger than quaternary alloys) have been conducted so far. On the theoretical side, the first theoretical reports on the pentanary alloys (with three composition variables) have been published very recently by Shim and Rabitz [8–10] using the universal tight binding model based on a modified pseudo-cell. Their investigations were undertaken in the pentanary alloy $Ga_xIn_{1-x}P_ySb_zAs_{1-y-z}$ of dimension $N = 3$ (*i.e.*, x, y and z). One reason for the paucity of experimental data for multi-component semiconductor alloys, with two composition variables and over, has been the lack of a systematic means to guide the experiments towards interesting regions of the composition space [2], whereas the scarcity of the theoretical work is mainly due to the computational difficulties and complexity.

The behavior of positrons in condensed matter has been the subject of intense experimental and theoretical investigation during the last decades, and the use of positrons can serve as a very efficient and sensitive probe of the electronic and atomic structure of materials [11–18]. In a typical experiment, positrons are injected into the target material either directly from a radioactive source or as a monoenergetic beam. Once injected the positrons rapidly lose their primary energy and being thermalized. The thermalized positrons diffuse through the sample until annihilation. The angular correlation of the two γ-rays resulting from the most probable decay process can be measured. In general, the interpretation of these measurements is facilitated by a computation of the momentum distribution of the two photons emitted in the annihilation process. Integration of this calculated two-photon (2γ) momentum distribution along a specified direction in momentum space yields a distribution that can be compared directly with the measured angular correlation. Since these photons are created by positron annihilation with electrons in a solid and the momentum distribution of the photons thus corresponds to that of the electrons, the angular correlation of positron annihilation radiations is considered to be a powerful method for studying the electronic structure of solids [19], because the positron mainly samples the valence electrons.

[a] e-mail: N_Bouarissa@yahoo.fr

Table 1. Band-gap energies of GaAs, InAs, GaSb, InSb, InP and GaP.

Compound	Band-gap energy (eV)					
	E_g^Γ		E_g^X		E_g^L	
	Exp.	EPM Calculations*	Exp.	EPM Calculations*	Exp.	EPM Calculations*
GaAs	1.42 [31]	1.42	1.81 [31]	1.81	1.72 [31]	1.72
InAs	0.36 [3]	0.36	1.37 [3]	1.37	1.07 [3]	1.07
GaSb	0.725 [32]	0.715	1.03 [33]	1.012	0.761 [33]	0.777
InSb	0.18 [3]	0.18	1.63 [3]	1.63	0.93 [3]	0.93
InP	1.35 [3]	1.35	2.21 [3]	2.21	2.05 [3]	2.05
GaP	2.78 [34]	2.774	2.26 [34]	2.25	2.6 [34]	2.6

* Present work

Up to now, the positron annihilation is successfully applied to investigate the electronic structure of elemental and compound semiconductors [20–28]. However, only limited studies have been reported on III-V ternary and quaternary alloys [29,30]. Moreover, to the best of our knowledge, positronic properties have never been previously reported for the pentanary semiconductor alloys. Thus, this paper is concerned with the theoretical study of the electronic and positronic properties in the pentanary semiconductor alloys $Ga_xIn_{1-x}P_ySb_zAs_{1-y-z}$ lattice matched to GaSb. The motivation for studying such alloys is that they are expected to provide more diverse opportunities to achieve desired band gaps while still maintaining the lattice matching conditions by controlling the composition components [2,9]. The purpose of this paper is to predict theoretical data for the band gaps of the alloy of interest which may serve to obtain the desired property and to determine for various compositions the positron band structure in particular the bottom of the lowest-energy band from which we extract the positron band effective mass and affinity that are important parameters for positron diffusion and preferential occupation or annihilation in semiconductors. We are also interested to calculate for different concentrations the electron-positron momentum densities along different directions and to deduce the corresponding percentage anisotropies. The shapes of the momentum distributions sensitively reflect the electronic states in the materials under investigation and hence their analysis may provide important microscopic information on these states. However, the calculations of these quantities need the knowledge of the electron and positron wave functions. For that, the electron wave functions are calculated using the empirical pseudopotential method (EPM) under the virtual crystal approximation (VCA) which found to be reliable for quaternary semiconductor alloys [6] when the compositional variations are taken into account. Because it is difficult to incorporate many-particle effects into the theory, the positron wave functions have been calculating in the point-core approximation for the ionic potential. We note that there is no exclusion principle between the electron and its anti-particle, the positron. The positron interactions are purely Coulombic in nature. We assume that there is only one positron in the sample at any time and hence there is no exchange part because there is no positron-positron interaction.

The organization of the paper is as follows. We explain the computational method in Section 2. The calculated results are presented and discussed in Section 3. We conclude the present work in Section 4.

2 Calculations

The electronic wave functions are obtained from the electronic band structure calculation that is based on the EPM, which involves the fitting of the atomic form factors to experiment. Therefore, the first step in this calculation is to find the best possible set of atomic form factors, which will describe well the band structure. The experimental energy band gaps at the principal symmetry points of the Brillouin zone used in the fitting procedure are given in Table 1. The final adjusted local symmetric and antisymmetric atomic form factors obtained from the optimization model [35] and used in our calculations, alongside with the lattice constants for GaAs, InAs, GaSb, InSb, InP, and GaP, are shown in Table 2.

The electron wave functions are expanded into plane waves,

$$\psi_{n,k}(r) = \left(\frac{1}{\Omega}\right)^{\frac{1}{2}} \sum_G C_{n,k}(G) \exp[\mathrm{i}(k+G)r] \qquad (1)$$

where Ω is the unit-cell volume and G is a reciprocal lattice vector. The cut-off energy of the plane waves is taken to be 14 Ry in the actual calculation.

It is straight forward to extend our treatment to alloys through the use of the VCA. Thus, for the multicomponent alloy which has the form $A_xB_{1-x}C_yD_zE_{1-y-z}$, the pseudopotential form factors are calculated according to the following expression,

$$\begin{aligned} V_{\mathrm{VCA}}(G) = {} & xy\,V_{\mathrm{AC}}(G) + xz\,V_{\mathrm{AD}}(G) + x(1-y-z)\,V_{\mathrm{AE}}(G) \\ & + (1-x)y\,V_{\mathrm{BC}}(G) + (1-x)z\,V_{\mathrm{BD}}(G) \\ & + (1-x)(1-y-z)\,V_{\mathrm{BE}}(G). \end{aligned} \qquad (2)$$

Table 2. Pseudopotential form factors obtained from the non linear least squares method and used lattice constants for GaAs, InAs, GaSb, InSb, InP and GaP.

Compound	Form factors (Ryd)						Lattice constant (Å)
	$V_S(3)$	$V_S(8)$	$V_S(11)$	$V_A(3)$	$V_A(4)$	$V_A(11)$	
GaAs	−0.239833	0.0126	0.059625	0.060536	0.05	0.01	5.653
InAs	−0.182147	0.00	0.047107	0.094714	0.05	0.03	6.058
GaSb	−0.191206	0.005	0.043533	0.045340	0.03	0.00	6.118
InSb	−0.201822	0.01	0.028443	0.064645	0.03	0.015	6.49
InP	−0.213862	0.00	0.070499	0.088818	0.06	0.03	5.869
GaP	−0.210510	0.03	0.072244	0.132668	0.07	0.02	5.451

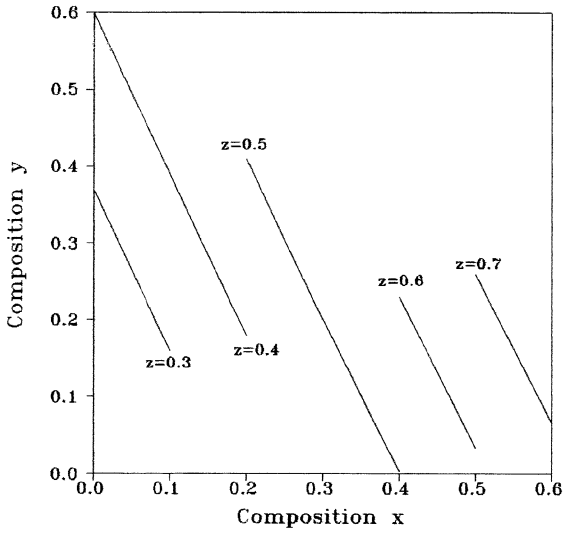

Fig. 1. Allowed lattice matching relations among x, y and z for the alloy $Ga_xIn_{1-x}P_ySb_zAs_{1-y-z}$ with the substrate GaSb.

The lattice constant $a(x, y, z)$ of the pentanary alloy is determined by using Vegard's law [36] as,

$$a_{\mathrm{ABCDE}}(x,y,z) = xy\,a_{\mathrm{AC}} + xz\,a_{\mathrm{AD}} + x(1-y-z)\,a_{\mathrm{AE}} + (1-x)y\,a_{\mathrm{BC}} + (1-x)z\,a_{\mathrm{BD}} + (1-x)(1-y-z)\,a_{\mathrm{BE}}. \quad (3)$$

The lattice matching conditions for the pentanary alloy $Ga_xIn_{1-x}P_ySb_zAs_{1-y-z}$ on GaSb substrate are as follows,

$$y = \frac{a_{\mathrm{sub}} - 0.033xz + 0.405x - 0.432z - 6.058}{-(0.013x + 0.189)} \quad (4)$$

where $a_{\mathrm{sub}} = a_{\mathrm{GaSb}} = 6.118$ Å.

The allowed lattice matching relations among x, y, and z for the alloy $Ga_xIn_{1-x}P_ySb_zAs_{1-y-z}$ with the substrate GaSb are shown in Figure 1.

For evaluating the positron potential, we have adopted the same approximation as that used in our previous paper [28], where the total ion charge is expressed as,

$$V_i^{\alpha}(r) = z_{\alpha}\frac{e^2}{r} \quad (5)$$

z_α is the valence charge of atom α, while the electron-positron Coulomb potential is taken as,

$$V_C(r) = -2\int \frac{\rho(r')}{|r-r'|}\mathrm{d}^3r'. \quad (6)$$

The positron gets pushed away from the ion core region into the interstitial positions, with its wave function vanishing at the ion core. This smooth structure of the positron wave function, which has no oscillations in the ion core region, lends itself very well to a representation in terms of a relatively small number of plane waves [37],

$$\psi_+(r) = \left(\frac{1}{\Omega}\right)^{\frac{1}{2}} \sum_G A(G)\exp(\mathrm{i}Gr) \quad (7)$$

where G is a reciprocal lattice vector. The coefficients $A(G)$ are found out by solving the positron secular equation.

The positron after coming to rest in the medium annihilates with the electrons giving rise to two photons, mostly emitted in directions opposite each other. The probability of annihilation of the electron-positron pair with momentum p is proportional to the pair momentum density,

$$\rho^{2\gamma}(p) = c\sum_{n,k}\eta_n(k)\left|\int \psi_{n,k}(r)\psi_+(r)\exp(-\mathrm{i}pr)\mathrm{d}^3r\right|^2. \quad (8)$$

Here c is a constant, $\psi_{n,k}(r)$ is the Bloch wave function for an electron with band index n and wave vector k and $\psi_+(r)$ is the ground state wave function of the positron corresponding to the wave vector $k = 0$, $\eta_n(k)$ is the occupation probability. In the present work, about 600 k points have been used to sample the Brillouin zone in each direction.

The long-slit angular correlation profile is represented as,

$$N(p_z) = \int_{-\infty}^{+\infty}\int_{-\infty}^{+\infty}\rho^{2\gamma}(p)\mathrm{d}p_x\mathrm{d}p_y. \quad (9)$$

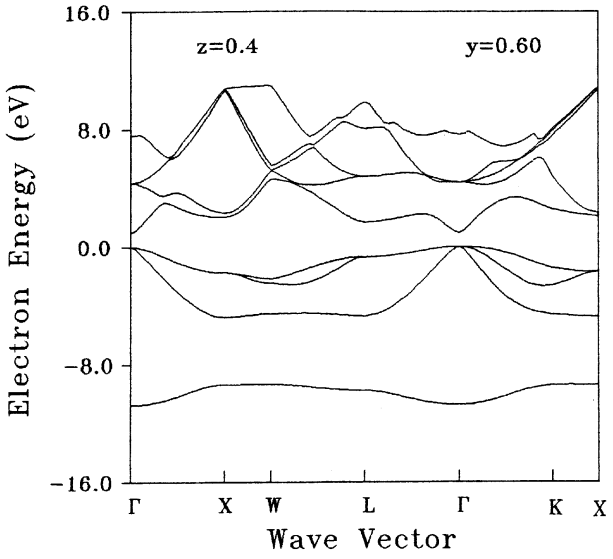

Fig. 2. Electron band structure for $Ga_xIn_{1-x}P_ySb_zAs_{1-y-z}$ lattice matched to GaSb.

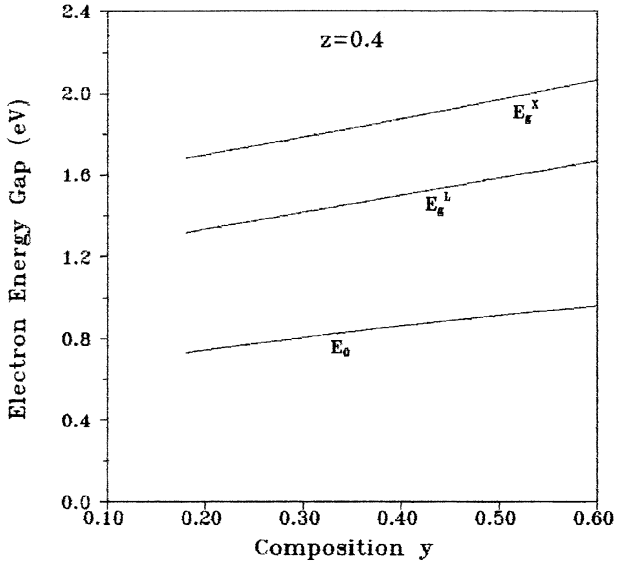

Fig. 3. Direct and indirect band-gap energies *versus* phosphorus composition in $Ga_xIn_{1-x}P_ySb_{0.4}As_{0.6-y}$ lattice matched to GaSb.

3 Results

3.1 Electronic structure and band gaps

Figure 2 displays the calculated electron band structure of $Ga_xIn_{1-x}P_ySb_zAs_{1-y-z}$ pentanary alloy for $z = 0.4$ and $y = 0.60$ lattice matched to GaSb along representative symmetrical directions of the Brillouin zone. The top of the valence band is taken as energy zero. The overall shape of the band structure seems to be similar to those of $Ga_{0.6}In_{0.4}P_{0.1}Sb_{0.1}As_{0.8}$ and $Ga_{0.6}In_{0.4}P_{0.7}Sb_{0.1}As_{0.2}$ [10] and that of $Ga_{0.2}In_{0.8}P_{0.5}Sb_{0.4}As_{0.1}$ lattice matched to InAs [38]. Both valence band maximum and conduction band minimum occur at the Γ high-symmetry point. Thus, the pentanary alloy of interest is a $\Gamma \rightarrow \Gamma$ direct – gap semiconductor with $E_g^\Gamma = E_0 = 0.96$ eV. Using the universal tight binding model based on a modified pseudocell, Shim and Rabitz [10] have reported a value of 0.901 eV for E_0 in the alloy system $Ga_xIn_{1-x}P_ySb_zAs_{1-y-z}$ (with $z = 0.4$, $y = 0.6$ and $x = 0.043$) lattice matched to GaSb. This value compares well with our obtained one. Recently Bouarissa *et al.* [38] have reported that there is a discrepancy between their results regarding the fundamental energy band gap of the pentanary alloy $Ga_{0.2}In_{0.8}P_{0.5}Sb_{0.4}As_{0.1}$ lattice matched to InAs and those reported in reference [10] for E_0 in $Ga_xIn_{1-x}P_ySb_zAs_{1-y-z}$ (with $z = 0.4$, $y = 0.5$ and $x = 0.181$) lattice matched to InAs. This discrepancy has been termed to be due to their calculations which neglected the effect of compositional disorder. We do conclude then that the effect of the latter on the present calculations is not as important as on $Ga_{0.2}In_{0.8}P_{0.5}Sb_{0.4}As_{0.1}$ lattice matched to InAs. Due to the fact that in our case $x \approx 0.0$ (the pentanary alloy of interest is lattice matched to GaSb with $z = 0.4$ and $y = 0.60$) which means that the material under study is a ternary alloy, on the contrary to the case when the alloy system is lattice matched to InAs with $z = 0.4$ and $y = 0.5$, where $x \approx 0.2$ (the material under investigation is a pentanary alloy), our results suggest that the compositional disorder is as important as the number of composition variables for the multi-component semiconductor alloys is higher.

In Figure 3, we have plotted the variation of the direct (E_0) and indirect (E_g^X and E_g^L) energy band gaps for the pentanary alloy of interest ($z = 0.4$) as a function of the composition y, with y varying from 0.18−0.6. All the band gap energies increase as the P concentration increases. Their behavior shows clearly that the absorption at the fundamental optical gaps in the alloy system under consideration is direct ($\Gamma \rightarrow \Gamma$) ranging in composition from $y = 0.18$ to $y = 0.6$. Qualitatively, the same behavior has been reported in reference [9]. From the quantitative point of view, our results show that the band gaps (E_g^Γ, E_g^X and E_g^L) of the alloy $Ga_xIn_{1-x}P_ySb_zAs_{1-y-z}$ lattice matched to GaSb with $z = 0.4$ and $y = 0.6$ are 0.96, 2.07 and 1.67 eV, respectively, which compare well with those of 0.901, 1.954 and 1.586 eV reported in reference [10]. It should be noted that the composition z may have other values rather than 0.4, provided that the allowed lattice matching relations among x, y and z for the alloy of interest are satisfied as shown in Figure 1. In these cases, the variation of y implies that the alloy under investigation provides more opportunities to obtain a desired band gap that could not be provided by ternary and quaternary alloys.

3.2 Positron band structure and related properties

The positron band structures for $z = 0.4$ and for different y compositions allowed by the lattice matching conditions for the alloy of interest along the representative

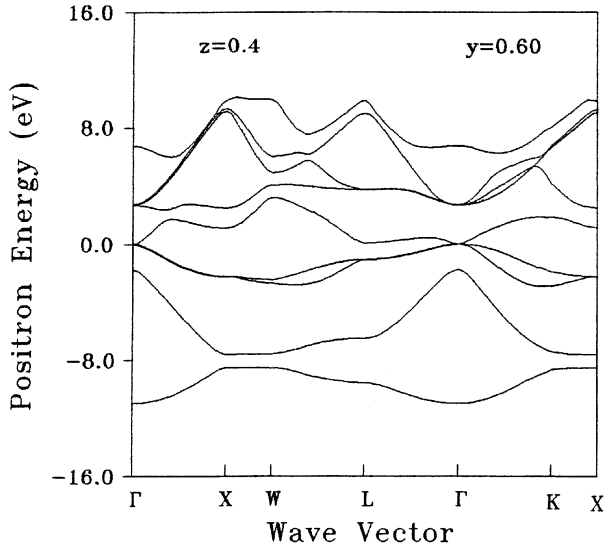

Fig. 4. Positron band structure for $Ga_xIn_{1-x}P_ySb_zAs_{1-y-z}$ lattice matched to GaSb.

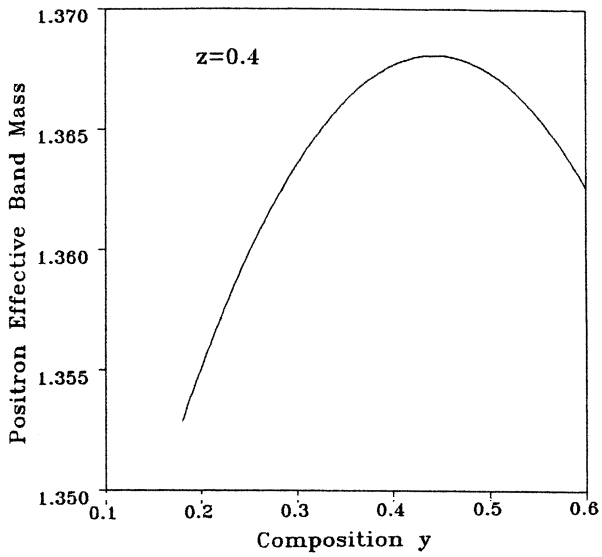

Fig. 5. Positron band effective mass *versus* phosphorus composition in $Ga_xIn_{1-x}P_ySb_{0.4}As_{0.6-y}$ lattice matched to GaSb.

symmetry lines of the Brillouin zone are computed. In order to facilitate the comparison with the electron band structure (Fig. 2), the zero energy reference is also taken to be at the top of the fourth band. We show just the curve for one y value ($y = 0.60$) (Fig. 4), since plots for the others were found to coincide (no differences among curves for three different values of y in the range 0.18−0.60 were visible). This may be due to the fact that the lattice constant is the same for all materials whatever the value of y, since the pentanary alloy of interest is lattice matched to GaSb. The picture is similar to those of the positron in III-V multi-component semiconductor alloys, with less than three composition variables [29,39,40] and resembles to that of the electron band structure (Fig. 2). Generally, the difference between positron band structures lies in the bottom of the lowest positron energy band at Γ state at $k = 0$, that corresponds to the positron thermalization energy, which has different values for different materials. Giving the fact that the positron thermalization time is short compared to its lifetime, the positron will annihilate in its fundamental energy state. The lowest positron band is rather free-particle-like and resembles closely the lowest valence electron one (Fig. 2).

The positron effective mass is an important parameter for studying positron diffusion in semiconductors. Strictly speaking, such a parameter can be obtained from the band structure of the material. As can be seen from Figure 4, the first positron band in the alloy of interest is almost perfectly parabolic and isotropic in the vicinity of its high- symmetry Γ_1-point. Thus, the effective band mass becomes scalar and is a value independent of a direction. Hence, it could be obtained simply by calculating the positron energy in few k points near the bottom of the lowest energy band and by taking the curvature,

$$m_b^* = \hbar^2 \left[\frac{\mathrm{d}^2 E}{\mathrm{d}k^2}\right]^{-1} \tag{10}$$

where m_b^* is the positron effective band mass and E is its energy.

Our results for m_b^* *versus* alloy composition y over the range 0.18−0.60 are shown in Figure 5. The variation of the positron effective band mass as a function of the y composition exhibits a non-linear behavior showing an upward effective band mass bowing. A least-squares fit of this curve gives the following analytical expressions,

$$m_b^*(y) = 1.32 + 0.19y - 0.22y^2. \tag{11}$$

The unit of the positron effective band mass is m_0, where m_0 is the positron free-particle mass. On going from $y = 0.18$ to $y = 0.60$, our calculated positron effective band mass lies in the range ∼1.353 m_0–1.367 m_0. Considering current experimental possibilities, it is not evident whether such a small change of the positron effective mass could be detected through studies of positron diffusion. Hence, we think that changing the P content in the alloy of interest with $z = 0.4$ does not affect much the positron effective mass. The latter has been estimated from experiments in few cases. However, the quantitative interpretation of the experimental results is not unambiguous. Therefore, the value of $m^* = 1.5\ m_0$ has been considered as a compromise over the various theoretical and experimental determinations [41]. A comparison between this value and our calculated ones, shows that the latter are smaller than that of 1.5 m_0. Such a discrepancy has been attributed according to Panda *et al.* in the case of Si [42] to the neglect of the positron-phonon and positron-plasmon interactions. It should be noted, however, that the largest contribution to the positron effective mass comes from the positron band effective mass, which agrees with the results of references [28,39,40,42].

Another interesting quantity that is related to the positron band structure is the positron affinity (A_+). The positron affinity reflects the preference of the positron for

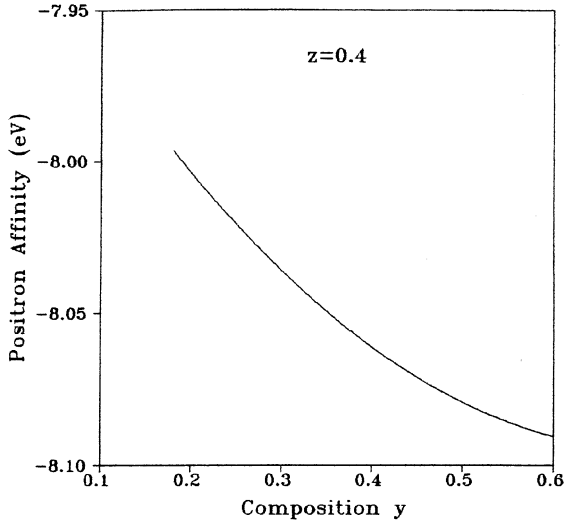

Fig. 6. Positron affinity *versus* phosphorus composition in $Ga_xIn_{1-x}P_ySb_{0.4}As_{0.6-y}$ lattice matched to GaSb.

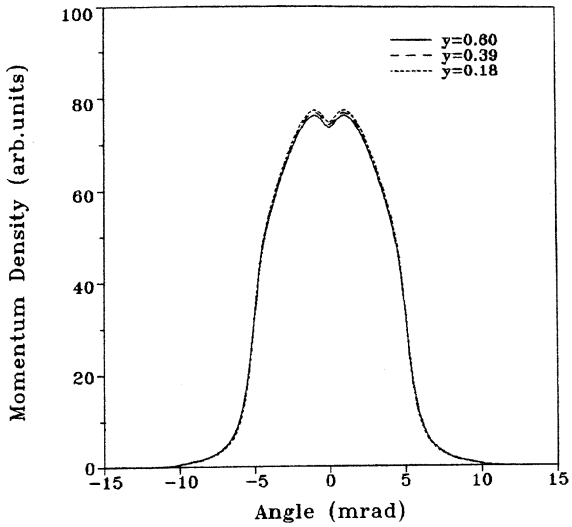

Fig. 7. The integrated electron-positron momentum densities in $Ga_xIn_{1-x}P_ySb_{0.4}As_{0.6-y}$ lattice matched to GaSb along the [110] direction.

Table 3. Predicted values of electron and positron chemical potentials, and positron affinity for $Ga_xIn_{1-x}P_ySb_zAs_{1-y-z}$/GaSb.

$(x,\ y,\ z)$	μ_-(eV)	μ_+(eV)	A_+(eV)
$(0,\ 0.6,\ 0.4)$	-0.48	-7.61	-8.09
$(0.1,\ 0.39, 0.4)$	-0.43	-7.63	-8.06
$(0.2, 0.18, 0.4)$	-0.37	-7.63	-8.00

different components in heterostructures made of different materials and the preference between the host matrix and precipitates in alloys [43]. Sometimes, however, A_+ is understood in terms of "attractivity" to positrons of different atoms inside materials containing more than one atomic component, or, in other words, preferential positron occupation or annihilation [44].

In our work, the positron affinity is defined by the simple relation [44],

$$A_+ = \mu_- + \mu_+ \tag{12}$$

where μ_- and μ_+ are the electron and positron chemical potentials, respectively. μ_+ may be identified with the positron thermalization energy, whereas μ_- is determined from the electron band structure and identified with the Fermi energy. Both μ_- and μ_+ are defined with respect to the same zero energy level. Table 3 shows quantitative predictive values of μ_-, μ_+ and A_+ for some compositions (x, y, z) in the pentanary alloy of interest. There is no experimental data to compare with, however, the calculated positron affinity for GaAs and GaP using the density functional theory with the electron energy in the local density approximation and the positron energy in the generalized gradient approximation, are found to be -7.90 and -7.95 eV, respectively [45]. We do believe then, that the order of magnitude of our calculated positron affinities is reasonable. The variation of the positron affinity *versus* alloy composition y in the range $0.18-0.60$ is plotted in Figure 6. In view of Figure 6, we note that the positron affinity decreases non-linearly with increasing y according to the following expression,

$$A_+(y) = -7.92 - 0.50y + 0.35y^2. \tag{13}$$

As a consequence, the positron has a more important affinity for low phosphorus concentrations (for $z = 0.4$) although, A_+ varies by about 1% in the studied concentration range. For example, for $Ga_xIn_{1-x}P_{y_1}Sb_zAs_{1-y_1-z}$ and $Ga_xIn_{1-x}P_{y_2}Sb_zAs_{1-y_2-z}$ in contact (with $y_1 < y_2$), the positron favours $Ga_xIn_{1-x}P_{y_1}Sb_zAs_{1-y_1-z}$ with a certain affinity difference. This affixity difference results mainly from the dipole step on the $Ga_xIn_{1-x}P_{y_1}Sb_zAs_{1-y_1-z}$-$Ga_xIn_{1-x}P_{y_2}Sb_zAs_{1-y_2-z}$ interface, because the chemical potentials for positrons are almost equal in these pentanary semiconductor alloys. Namely, if a few layers of $Ga_xIn_{1-x}P_{y_2}Sb_zAs_{1-y_2-z}$ are grown on $Ga_xIn_{1-x}P_{y_1}Sb_zAs_{1-y_1-z}$, the positronium emission out of the sample is strongly reduced in comparison to the case when the sample is prepared by growing $Ga_xIn_{1-x}P_{y_1}Sb_zAs_{1-y_1-z}$ on $Ga_xIn_{1-x}P_{y_2}Sb_zAs_{1-y_2-z}$.

3.3 Electron-positron momentum densities

In Figures 7 and 8, we show the profiles of the integrated electron-positron momentum densities for various y compositions in the alloy of interest along the [110] and [001] directions, respectively. In view of Figure 7, one can note that the electron-positron momentum densities along the [110] direction for the materials under study are seen to be peaked. Compared with this, the profiles along the [001] direction are found to be flat (Fig. 8). This behavior is quite similar to the corresponding data in multi-component semiconductor alloys with less than three composition variables [29,30]. The peaking and the flatness in the profiles along the [110] and [001] directions could be understood in terms of the contributions from σ- and π-bonding orbitals to the ideal sp^3 hybrid bands. It

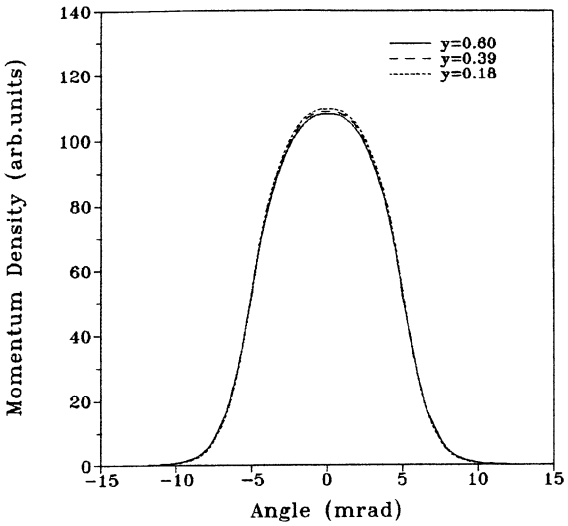

Fig. 8. The integrated electron-positron momentum densities in $Ga_xIn_{1-x}P_ySb_{0.4}As_{0.6-y}$ lattice matched to GaSb along the [001] direction.

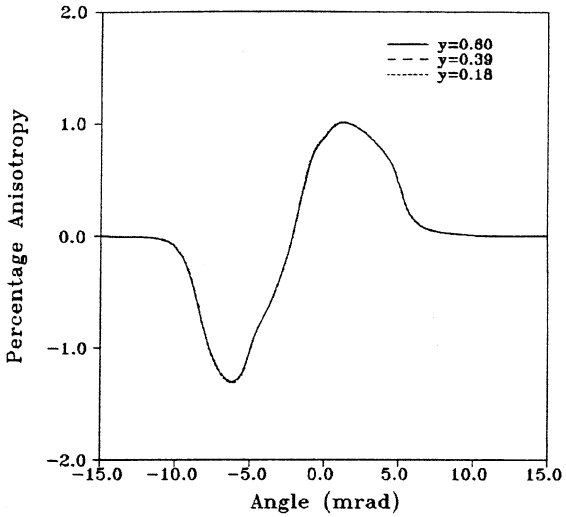

Fig. 9. Percentage anisotropy of the momentum densities in $Ga_xIn_{1-x}P_ySb_{0.4}As_{0.6-y}$ lattice matched to GaSb.

is interesting to see how these momentum density profiles are affected when going from the composition $y = 0.18$ to the one of $y = 0.60$ (Figs. 7 and 8). It seems that increasing the composition y manifests by a decrease of the fractional area of the momentum density along both studied directions. This in itself leads to a decrease in the total positron annihilation rate which in turn leads to an increase in the positron lifetime. The decrease of the annihilation rate is mainly due to the decrease in the valence contribution since the pseudopotential method reflects only the low momentum components. We do think that the refinement of the calculations making allowance for the core contributions would not change the results significantly because the positron avoids the ion-core region. The fact that the values of the momentum density becomes larger when the composition y becomes smaller may be due to the valence orbitals that are comparatively more diffused for small compositions y for their corresponding smaller band-gap energy. It should be noted that the variation of the composition y does not affect significantly the shape of the peaking and flatness. According to reference [29], the lattice constant and the bonding strengths combine to alter the shape of the momentum density data. Since in our case the lattice constant does not change whatever the value of y (the material of interest is lattice matched to GaSb), we do believe that the change of the composition y does not affect significantly the bonding strengths of the σ and π bands.

In order to observe the crystalline effect, it is convenient to check the anisotropy. The percentage of anisotropy parameter ε is defined as,

$$\varepsilon = \frac{[\rho_{[001]}(p) - \rho_{[110]}(p)]}{\rho_{[001]}(0)}. \qquad (14)$$

The percentage anisotropies for different compositions y ranging from $y = 0.18$ to $y = 0.60$ for $Ga_xIn_{1-x}P_ySb_{0.4}As_{0.6-y}$ with the substrate GaSb are shown in Figure 9. The results are seen to resemble those obtained in case of Ge [46]. However, compared to Ge, we find a somewhat lower magnitude of the peak for the alloy of interest. This may be because of the ionicity of $Ga_xIn_{1-x}P_ySb_{0.4}As_{0.6-y}$/GaSb which gives rise to a smaller anisotropy. Based on group theory, Saito *et al.* [21] have showed recently that the symmetry in the case of GaAs (III-V semiconductor compound) is lowered from O_h^7 in the case of Si to T_d^2. The two atoms in each unit cell are inequivalent to each other, and the number of symmetry operations is thus decreased from 48 to 24. Since the glide and screw operations are not included in this space group, these crystals are symmorphic. In view of Figure 9, one can notice also the negative value in the low momentum region of the anisotropy. The latter is believed to be due to the anisotropic positron wave function which samples the electron density differently along different directions since according to Panda *et al.* [47] the Compton profile data of III-V semiconductors show a positive anisotropy. It seems that increasing the composition y over the range 0.18 to 0.60 has no significant effect on the percentage anisotropy.

4 Conclusion

We have investigated the electronic and positronic properties of the pentanary semiconductor alloys $Ga_xIn_{1-x}P_ySb_zAs_{1-y-z}$/GaSb (with $z = 0.4$). The dependences on phosphorus concentration y ($0.18 \leq y \leq 0.6$) of several electronic and positronic quantities such as, band structure, energy gaps, effective band mass, affinity, momentum densities and percentage anisotropy have been predicted.

Generally our results regarding the electronic properties of the alloy of interest compared well with those obtained from the universal tight binding model based on

a modified pseudocell. Although no experimental data regarding the electronic properties of the alloy under consideration are available for the time being, our results suggest that the alloy $Ga_xIn_{1-x}P_ySb_zAs_{1-y-z}$/GaSb could provide additional opportunities to obtain a desired band gap beyond that available from quaternary alloys. This ability to tailor the materials makes them candidates for microelectronic engineers in their work on the design of III-V multi-component semiconducting materials with special features and properties. On the other hand, while most of the predicted positronic properties are understandable qualitatively which provides a new insight into the physics of the positron diffusion and annihilation in III-V pentanary semiconductor alloys, their quantitative behavior seems to be difficult to be verified experimentally due to the small change exhibited by the positronic quantities.

Part of this work has been done at the Max-Planck Institute for Physics of Complex Systems (MPI-PKS), Dresden, Germany. The author gratefully acknowledges the financial support from the MPI-PKS and expresses his sincere thanks to the MPI-PKS staff for their kind hospitality during his stay at the Institute.

References

1. I. Vurgaftman, J.R. Meyer, L.R. Ram-Mohan, J. Appl. Phys. **89**, 5815 (2001) and references cited therein
2. H. Rabitz, K. Shim, J. Chem. Phys. **111**, 10640 (1999) and references cited therein
3. S. Adachi, J. Appl. Phys. **61**, 4869 (1987) and references cited therein
4. N. Bouarissa, Phys. Lett. A **245**, 285 (1998)
5. K. Shim, H. Rabitz, Phys. Rev. B **57** (1998) 12874
6. N. Bouarissa, Superlattices and Microstructures **26**, 279 (1999)
7. K. Kassali, N. Bouarissa, Microelectronic Engineering **54**, 277 (2000)
8. K. Shim, H. Rabitz, Phys. Rev. B **58**, 1940 (1998)
9. K. Shim, H. Rabitz, J. Korean. Phys. Soc. **34**, S28 (1999)
10. K. Shim, H. Rabitz, J. Appl. Phys. **85**, 7705 (1999)
11. S. Berko, in *Momentum Distributions*, edited by R.N. Silver, P.E. Sokol (Plenum Press, New York, 1989), p. 273 and refrences cited therein
12. M.J. Puska, R.M. Nieminen, Rev. Mod. Phys. **66**, 841 (1994)
13. A. Dupasquier, A.P. Mills Jr., *Positron Spectroscopy of Solids*, edited by A. Dupasquier, A.P. Mills Jr. (IOS Press, Amsterdam, 1995)
14. A.A. Manuel, R. Ambigapathy, P. Hautojarvi, K. Saarinen, C. Corbel, J. Phys. IV, Colloq., Suppl. J. Phys. III **5**, C1-73 (1995)
15. B. Barbiellini, M. Hakala, M.J. Puska, R.M. Nieminen, A.A. Manuel, Phys. Rev. B **56**, 7136 (1997)
16. A. Rubaszek, Z. Szotek, W.M. Temmerman, Phys. Rev. B **63**, 165115 (2001)
17. A. Rubaszek, Z. Szotek, W.M. Temmerman, Mater. Sci. Forum **363**, 603 (2001)
18. A. Rubaszek, Z. Szotek, W.M. Temmerman, Phys. Rev. B **65**, 125104 (2002)
19. S. Berko, in *Positron Solid State Physics*, W. Brandt, A. Dupasquier (North Holland, Amsterdam, 1983), p. 64
20. B.K. Panda, D.P. Mahapatra, H.C. Padhi, K.P. Gopinathan, C.S. Sundar, G. Amarendra, J. Phys. C **21**, 6039 (1988)
21. M. Saito, A. Oshiyama, S. Tanigawa, Phys. Rev. B **44**, 10601 (1991)
22. B.K. Panda, D.P. Mahapatra, H.C. Padhi, Phys. Stat. Sol. (b) **167**, 133 (1991)
23. B.K. Panda, H.C. Padhi, B. Viswanathan, Phys. Stat. Sol. (b) **173**, 621 (1992)
24. H. Kondo, Y.-K. Cho, T. Kubota, T. Kawano, K. Watanabe, S. Tanigawa, J. Phys. Cond. Matt. **4**, 5911 (1992)
25. B.K. Panda, Phys. Rev. B **49**, 2521 (1994)
26. W. LiMing, B.K. Panda, S. Fung, C.D. Beling, J. Phys. Cond. Matt. **9**, 8147 (1997)
27. Z. Tang, M. Hasegawa, T. Chiba, M. Saito, H. Sumiya, Y. Kawazoe, S. Yamaguchi, Phys. Rev. B **57**, 12219 (1998)
28. N. Bouarissa, J. Phys. Chem. Solids **61**, 109 (2000) and references cited therein
29. N. Bouarissa, Philos. Mag. B **80**, 1743 (2000)
30. N. Bouarissa, Modern. Phys. Lett. B **13**, 599 (1999)
31. D.E. Aspnes, C.G. Olson, D.W. Lynch, Phys. Rev. Lett. **37**, 766 (1976)
32. S. Zollner, M. Garriga, J. Humlicek, S. Gopalan, M. Cardona, Phys. Rev. B **43**, 4349 (1991)
33. C. Alibert, A. Joullie, A.M. Joullie, C. Ance, Phys. Rev. B **27**, 4946 (1983)
34. *Handbook Series on Semiconductor parameters*, Vol. 1, edited by M. Levinshtein, S. Rumyantsev, M. Shur (World Scientific, 1996)
35. T. Kobayasi, H. Nara, Bull. Coll. Med. Sci., Tohoku Univ. **2**, 7 (1993)
36. L. Vegard, Z. Phys. **5**, 17 (1921)
37. B.K. Panda, D.P. Mahapatra, J. Phys. Cond. Matt. **5**, 3475 (1993)
38. N. Bouarissa, H. Baaziz, Z. Charifi, Phys. Stat. Sol. (b) **231**, 403 (2002)
39. N. Bouarissa, Z. Charifi, Mater. Chem. Phys. **53**, 179 (1998)
40. N. Bouarissa, J. Phys. Chem. Solids **62**, 1163 (2001)
41. O.V. Boev, M.J. Puska, R.M. Nieminen, Phys. Rev. B **36**, 7786 (1987)
42. B.K. Panda, Y.Y. Shan, S. Fung, C.D. Beling, Phys. Rev. B **52**, 5690 (1995)
43. M.J. Puska, P. Lanki, R.M. Nieminen, J. Phys, Cond. Matt. **1**, 6081 (1989)
44. J. Kuriplach, M. Sob, G. Brauer, W. Anwand, E.-M. Nicht, P.G. Coleman, N. Wagner, Phys. Rev. B **59**, 1948 (1999)
45. B.K. Panda, G. Brauer, Acta Physica Polonica A **95**, 641 (1999)
46. N. Bouarissa, T. Kobayasi, H. Nara, H. Aourag, Solid State Commun. **96**, 689 (1995)
47. B.K. Panda, D.P. Mahapatra, H.C. Padhi, Phys. Stat. Sol. (b) **169**, 89 (1992)